Asian Journal of Chemistry; Vol. 37, No. 6 (2025), 1322-1330

ASIAN JOURNAL OF CHEMISTRY

https://doi.org/10.14233/ajchem.2025.33670

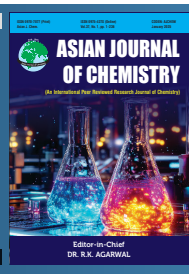

Green Synthesis of Cu-Zn Bimetallic Nanoparticles *via Trifolium alexandrinum* Extract: Structural Characterization, Biochemical Potential and Photocatalytic Application

NIRANTAK KUMAR[1], ANITA RANI[1,*], MANOJ KUMAR[2,*], POOJA DHIMAN[3], SHASHI SHARMA[4], HARDEEP SINGH TULI[5] and PALLVI AGGARWAL[6]

[1]Department of Chemistry, IEC University, Baddi, Solan-174103, India
[2]Department of Chemistry, Maharishi Markandeshwar University, Sadopur, Ambala-134007, India
[3]Department of Chemistry, Maharaja Agrasen University, Baddi, Solan-174103, India
[4]Toxicology Division, Forensic Science Laboratory, Madhuban, Karnal-132037, India
[5]Department of Bio-Technology, Maharishi Markandeshwar (Deemed to be) University, Mullana, Ambala-133207, India
[6]Department of Chemistry, Pt. C.L.S. Government College, Karnal-132001, India

*Corresponding authors: E-mail: caoudhary.anita@gmail.com; manojraju27@gmail.com

Received: 2 March 2025; *Accepted*: 22 April 2025; *Published online*: 27 May 2025; AJC-22004

The goal of this study was to synthesize the bimetallic nanoparticles using leaf extract of *Trifolium alexandrinum*, copper sulphate and zinc sulphate and screening their biological and photocatalytic activities. Since growing antibiotic resistance is a significant problem, metallic nanoparticles, which are well-known for their wide biological spectrum, are proving to be an efficient substitute for currently available antibiotics. Leaf extract of *T. alexandrinum* (TFL) and its bimetallic Cu-Zn (CZS) nanoparticles have been synthesized. Fourier transform infrared spectroscopy, ultraviolet spectroscopy, transmission electron microscopy, field emission scanning electron microscopy, X-ray diffraction and energy dispersive X-ray were used to analyze and characterize the synthesized nanoparticles. The Fourier transform infrared spectroscopy describes the presence of different functional groups in the leaf extract as well as changes in their nature after combining with metal salts. Field emission scanning electron microscopy reveals the formation of nanoparticles in agglomerated form with spherical shape. Transmission electron microscopy images also coincide with the results of scanning electron microscopy. The X-ray diffraction pattern confirms the formation of crystalline nanoparticles with 77% crystallinity with an average size of about 50-150 nm, whereas EDX certifies the presence of different constituent abundances in the form of percentage. Further, the biological potential of the obtained nanoparticles was estimated by evaluating the antimicrobial and anti-angiogenic activities. The maximum value for bacterial inhibition was found to be 21.5 mm and for fungal inhibition this value reaches to 20 mm for 100 µL each. The percentage inhibition on vessel growth rate in TFL/CZS nanoparticle treated groups was obtained as 28% (1 µg) and 85% (10 µg). Percentage degradation for the composite was attained 83%, which was much better than CZS nanoparticles towards the Congo red dye. Results have shown that subjected nanoparticles were proven as excellent biological agents. Moreover, the photocatalytic activity confirms that the novel bimetallic nanoparticles can be used to treat the wastewater at initial level.

Keywords: *Trifolium alexandrinum* Leaf extract, Bimetallic nanoparticles, Photocatalysis, Anti-angiogenesis, Antimicrobial activity.

INTRODUCTION

Researchers in several fields, including chemistry, medicine, biotechnology and pharmaceuticals, have taken a keen interest in nanoparticles in recent decades due to their enormous potential uses [1,2]. Moreover, nanoparticles also play very interesting roles in other areas like power generation, environmental science, computing areas and optics, *etc.* [3]. A wide range of physical, chemical, and ecologically benign methods known for the synthesis of nanoparticles. Due to the numerous disadvantages of physical and chemical methods, such as their high cost, use of hazardous chemicals, lengthy processing times, laborious procedures and many more, there is a need for some techniques that can produce quick synthesis and eco-friendly approaches to synthesized required nanoparticles [4,5]. In this regard, the green approach of synthesizing nanoparticles utilizing extracts from various plant parts has been used, which is thought to be a cost-effective, non-toxic, easy and eco-friendly method [6,7].

An improvement in nanoparticle efficiency due to complexation has made the incorporation of metals like gold, copper, zinc, silver, and nickel into plant extracts to form nanoparticles one of the most fascinating research opportunities over the past decade [8-10]. Currently, researchers are exploring the potential of two distinct metals merging to create bimetallic nanoparticles. Two different aqueous solutions of metal salts are frequently combined with plant extract to produce bimetallic nanoparticles. According to some theories, metals in these reactions combine with plant phytochemicals that have oxidizing or reducing properties to create nanoparticles [11,12]. It has been found that metal ions with greater reducing power reduce more quickly than those with less reduction potential. The biological characteristics enhance with the introduction of a single metal and improve significantly more rapidly with the addition of another metal.

Different plants from the genus *Trifolium* have been used traditionally for different applications. Some species are used in the form of antiseptics, analgesics, antimicrobials and to treat rheumatic aches. One common species of *Trifolium* with name the *alexandrinum* is well known for its tremendous antibacterial activity [13]. Earlier the investigation of phytochemicals in this plant indicates the presence of amino acids along with their derivatives, flavonoids, fatty acids, isoflavonoids, glycosides and different proteins [14,15]. The intake of flower extract of this plant along with water and hexane is found to decrease the glucose level and increase the insulin level in male rats, hence can be used to cure diabetes.

The synthesis of bimetallic nanoparticles from *Trifolium alexandrinum* leaf extract is revealed in the presented study. The production of metallic nanoparticles is thought to be easier, less expensive, safer, quicker and simpler than using traditional procedures since the plant's leaf extract has a great reduction potential due to the presence of the phytochemicals [16]. To obtain bimetallic nanoparticles (TFL/CZS), Cu-Zn metals were added to the leaf extract, resulting in the formation of bimetallic nanoparticles. The biological activities of the synthetic bimetallic nanoparticles, particularly its antibacterial and anti-angiogenic characteristics, were also evaluated. Moreover, the photocatalytic activity of these bimetallic-based nanoparticles was examined utilizing Congo red dye.

EXPERIMENTAL

The AR grade zinc and copper sulphate were acquired from Merck, USA. Each reaction was carried out using a hot plate and a magnetic stirrer. From the Institute of Microbial Technology (IMTECH) located in Chandigarh, procured the Microbial Type Collection Culture (MTCC). Throughout the entire testing phase, double-distilled water was used. To avoid any contamination, all equipments were thoroughly cleaned using double-distilled water and dried in a hot air oven.

Preparation of leaf extract of *Trifolium alexandrinum* (TFL): The preparation of leaf extract of *T. alexandrinum has* been done by absorption application and UV-readings [17,18]. Fresh leaves of *T. alexandrinum* were identified and collected from local area of Panchkula city, India. The leaves were washed with tap water and followed by doube distilled water. After washing, leaves were dried in shade for 10 days and then converted to fine powder using an electric grinder. Leaves powder (15 g) were mixed with 100 mL of water in 200 mL beaker at room temperature, incubated at 25 ºC for 24 h and then the content was stirred for 30 min at room temperature by using a magnetic stirrer. The obtained dark brown coloured content was filtered by using Whatman No. 1 filter paper. The filtrate was collected in a beaker and preserved at 4 ºC in a refrigerator for further processes.

Preparation of bimetallic Cu-Zn nanoparticles (CZS): Stirred each 50 mL of freshly prepared zinc sulphate (0.1 M) and copper sulphate (0.1 M) solutions while using a magnetic stirrer for 2 h followed by the addition of 10% NaOH solution dropwise under stirring. The pH was maintained up to 9 and monitored. As the solution was obtained, a sapphire-coloured precipitates appeared. After 2 h of stirring, the precipitate was filtered and dried in a vacuum desicator overnight.

Preparation of leaf extract based bimetallic Cu-Zn nanoparticles (TFL/CZS): A 50 mL of total solution (25 mL each of copper sulphate and zinc sulphate) was taken collectively and added dropwise to 25 mL of leaf extract solution. The pH of the whole solution was maintained at 9-10 by dropwise addition of NaOH solution while stirring for 2 h using magnetic stirrer at 25 ºC. The colour of the solution turns dark brown to parrot green, which confirm the formation of bimetallic Cu-Zn nanoparticles. After that the mixture was allowed to stand undisturbed at room temperature for approximately 1 h. The fine precipitate was dried slowly on a petri plate in a hot oven at 25 ºC. The dried bimetallic nanoparticles were washed with water several times with centrifugation. The obtained green precipitate was again dried and utilized for further processing.

Characterization: The FETEM JEM 2100 plus was used to conduct the TEM analysis followed by FESEM and EDX analysis on Hitachi, Japan, SU8010 series. On the other hand, the XRD characterization was conducted on the PANalytical X'Pert PRO diffraction with Cu*K*α radiation at Advanced Material Research Centre, IIT Mandi. On the other hand, the molecular structure of the obtained nanoparticles was analyzed using FTIR on Perkin-Elmer using KBr pallet ranging between 4000-400 cm^{-1} at Lovely Professional University, Punjab.

Antimicrobial activity: The agar well-diffusion method was deployed in triplicate (n = 3) to measure the antifungal and antibacterial activities of the synthesized leaf extract based bimetallic (TFL/CZS) nanoparticles. Nutrient agar plates were cultivated with 100 µL bacteria and fungi culture by using an L-shaped spreader and wells of appropriate and the same diameter were measured. DMSO was used to prepare the solutions of TFL/CZS due to the complete solubility of latter in the former. Solutions of 10, 25, 50 and 100 µg/mL of TFL/CZS were prepared and subjected to evaluate antibacterial activity against bacteria *viz. Salmonella typhi*, *Bacillus subtilis* and fungi *Aspergillus niger*, *Trichophyton rubrum.* The common antibiotic drug chloramphenicol and antifungal drug *i.e.* fluconazole were taken as standard to compare the antimicrobial activity of tested compound. After incubating the samples at 37 ºC for 24 h, the inhibitory zones were identified on the plates [19,20]. The complete inhibition activity was observed after 48 h of incubation to obtain the maximum activity.

Anti-angiogenic activity

Chorioallantoic membrane (CAM) assay: CAM assay was applied to evaluate the anti-angeogenic activity of the synthesized nanoparticles, *i.e.* TFL/CZS and CZS alone. The cleaned, fertilized chicken eggs were collected and kept in a chamber containing 70% humidity and 37 ºC temperatures. Albumin (1 mL) was removed from the lower side of the eggs with a surgical syringe. After 48 h and the pierced holes were covered with a sterilized laboratory tape. A small window was created by removing the egg shell at the blunt end after 72 h of incubation. After confirmation of viable and normal development of embryo, different concentrations of TFL/CZS and TFL (*i.e.* 0, 1 and 10 µg) were loaded on 5 mm sterilized filter discs and then kept over the surface of the extra embryonic membrane. The windows were again sealed with sterilized laboratory tape to block the contact with the external environmental and eggs were placed for 48 h under incubation. After the treatment, the antiangiogenic effect of applied compounds was manually counted in terms of branch points over CAM and the percent inhibition was calculated as follows:

$$\text{Inhibition (\%)} = \frac{\text{Data of control} - \text{Data of treated}}{\text{Data of control}} \times 100$$

Photocatalytic activity: The photocatalytic degradation capability of TFL/CZS was examined for the degradation of Congo red dye under solar illumination. The photocatalytic activity was carried out by a double walled glass chamber of Pyrex. A 1×10^{-5} M solution of Congo red dye was added to 50 mg of nanoparticles at 30 ± 1 ºC. The adsorption-desorption equilibrium was mixture was achieved by keeping the whole solution in dark. After that, the solution was irradiated under sunlight and 3 mL of aliquot were taken out at different time intervals *i.e.* 0, 30, 60, 90, 120, 150 and 180 min. The absorbance of all solutions with different concentrations was subjected to ultraviolet spectrophotometry and absorbance was noted at the specified wavelengths [21]. The percentage degradation of dye was calculated using the formula as:

$$\text{Degradation (\%)} = \frac{C_o - C_t}{C_o} \times 100$$

where C_o = initial concentration and C_t = instant concentration of dye sample.

The kinetics of degradation was explained by pseudo-first-order kinetics. The rate constant (k) was calculated by the following equation:

$$k = \frac{[A]_o / [A]_t}{t}$$

where the slope obtained from the plot of ln A_o/A *vs.* t.

Further different parameters like the effect of pH of the solution, photocatalyst dosage and concentration of dye were studied and degradation efficiency was calculated.

RESULTS AND DISCUSSION

The standard curve was prepared to analyze the concentration of the TFL/CZS in preparation of the mixture. The synthesized nanoparticles (TFL/CZS) absorbed the most at 236 nm (max) in this preparation. The plot of nanoparticles concentration *vs.* absorbance for synthesis is shown in Fig. 1.

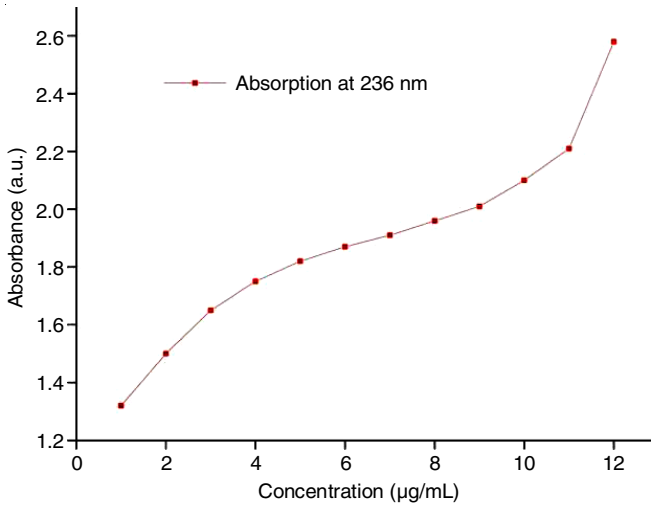

Fig. 1. Plot of nanoparticles concentration *vs.* absorbance

FTIR spectral studies: Fig. 2 describes the characteristics peaks for corresponding functional group present in the organic part (TFL) and corresponding nanoparticles (TFL/CZS). FTIR spectrum of *T. alexandrinum* leaf powder depicted broad band at 3278 cm^{-1} representing the hydroxyl (-OH) group [22]. While the band at 1641 cm^{-1} can be assigned to the aromatic bending of carbonyl group (*i.e.* -C=O) [23]. The peak at 1046 cm^{-1} corresponds to the stretching vibration of (C-O), which confirms the presence of carbonyl group in the extract. A careful observation of spectrum of bimetallic nanoparticles of *T. alexandrinium* shows the absence of broad band at 3288 cm^{-1} which indicate the involvement of hydroxyl oxygen in the coordination with the metal atoms. Similarly shifting of all other bands to lower values shows the effect of involvement of metal atoms in the organic moiety. Formation of Cu-Zn nanoparticles is confirmed by presence of strong band at 508 cm^{-1} and 435 cm^{-1} which may be due to Cu-O and Zn-O stretching vibrations, respectively [24-26]. Quantification of FTIR peak intensities was conducted to compare the functional group interactions before and after

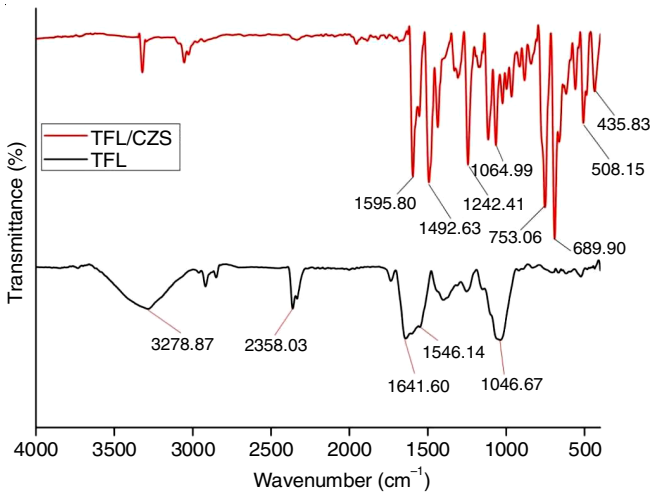

Fig. 2. FTIR spectra of TFL and TFL/CZS nanoparticles

nanoparticle formation. Moreover, the statistical analysis was performed where applicable, using mean ± standard deviation (SD) for peak intensity variation.

SEM and EDX studies: The surface morphology of the leaves powder, bimetallic nanoparticles and metal based leaf nanoparticles was studied and compared by using scanning electron microscopy (SEM). Fig. 3a-f represent the detailed information regarding SEM images of all the tested materials. SEM images 3a and 3b shows the irregular shape of the organic part alone *i.e.* TFL, while images 3c and 3d are of nanoparticles obtained from inorganic salt mixture *i.e.* CZS. On the other hand, SEM image of TFL/CZS (3e and 3f) revealed well-shaped nanoparticles with exhibiting spherical geometry. The TFL/CZS nanoparticles were found to form agglomerates with a particles size ranging from 50-150 nm, which indicate the tendency of nanoparticles to form clusters.

To obtain the maximum information about the synthesized nanoparticles, the analysis was also performed by using EDX technique. Quantification of elemental composition was performed using atomic percentage (%) and weight percentage (%) calculation for each detected element. The standard deviation (SD) values were calculated for repeated measurement to ensure the consistency.The presence of each and individual elements are shown in Fig. 4 along with particular amount (Table-1). The total weight percentage of the analyzed component sums up to 71.24 wt.% with carbon and oxygen being the major element present in the sample.

TABLE-1
ELEMENTAL ANALYSIS OF TFL/CZS

Element	Unn. (wt.%)	C norm. (wt.%)	C atom. (wt.%)	C error (3σ) (wt.%)
Carbon	16.13	22.65	43.69	7.98
Oxygen	16.84	23.64	34.24	7.27
Zinc	17.04	23.95	8.48	2.17
Copper	15.19	21.33	7.78	1.82
Sulfur	4.38	61.15	4.44	0.57
Potassium	1.64	2.31	1.37	0.26
Magnesium	0.00	0.00	0.00	0.00
Total	71.24	100.00	100.00	

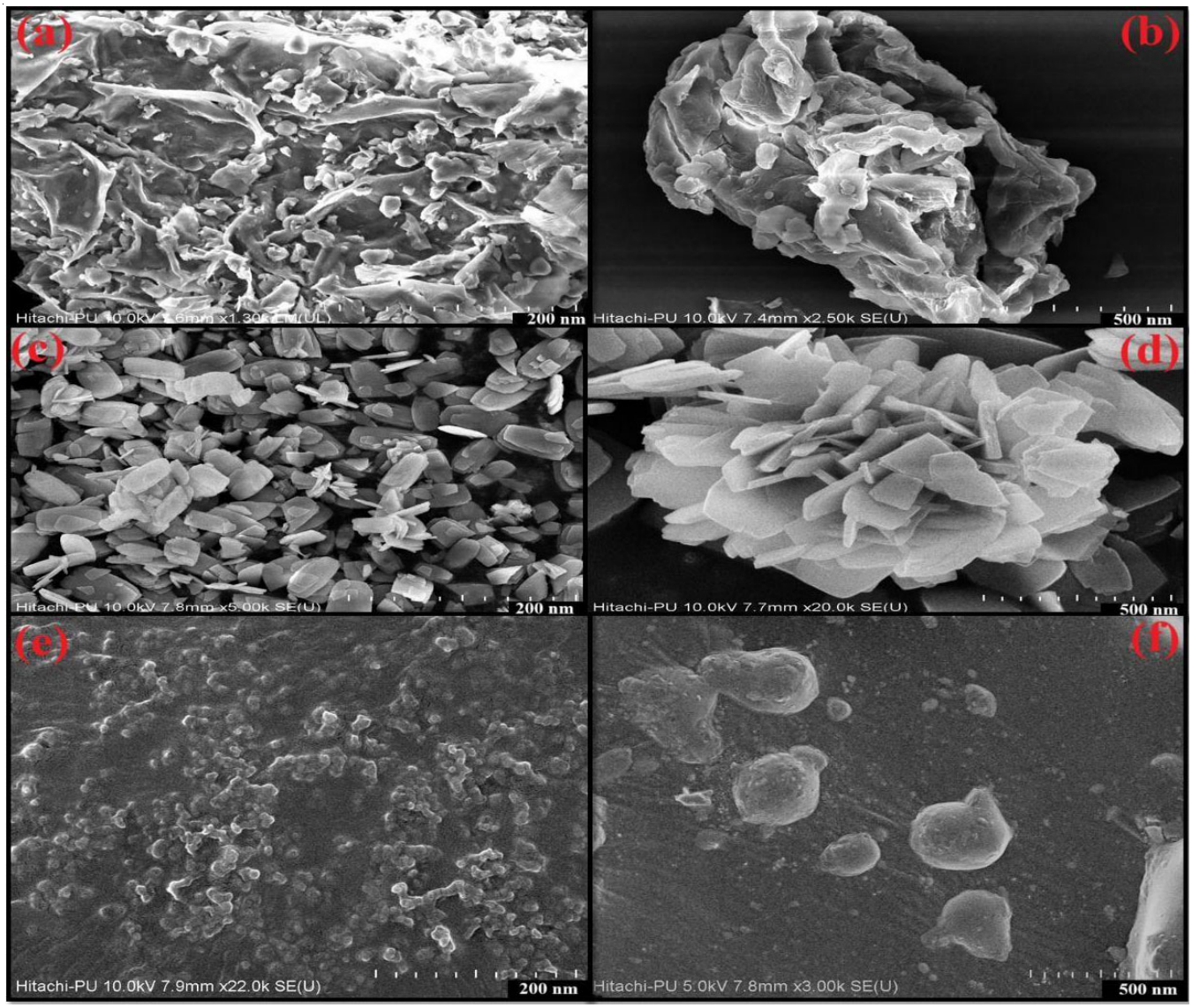

Fig. 3. SEM images of TFL (a-b), CZS (c-d) and TFL/CZS (e-f)

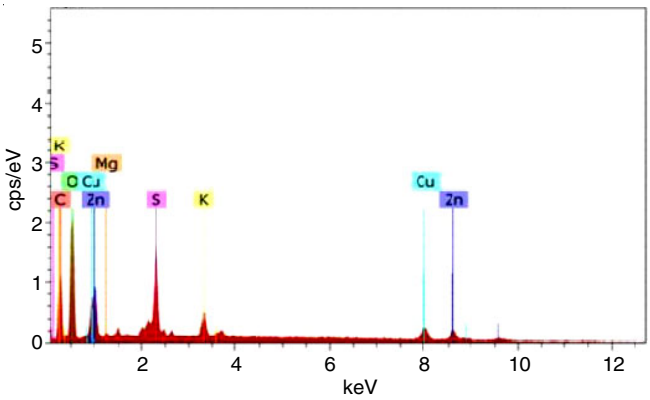

Fig. 4. EDX image of TFL/CZS

TEM studies: The TEM micrograph (Fig. 5) displayed images of $ZnSO_4$ and $CuSO_4$ nanoparticles in proximity, suggesting a strong likelihood of interfacial hetero-junction formation due to lattice fringe separation [27]. These images confirmed the agglomeration of all the involved moieties to form the nanoparticles as no separate boundaries are visible for organic or inorganic part.

XRD studies: The XRD spectrum of powder TFL exhibited a single broad peak at 22.01º, indicating its predominantly amorphous nature with crystallinity of only 8%. This suggests that the material is highly disordered. On the other hand, in case of CZS, sharp peaks were observed at 16.7º, 22.07º, 28.11º, 33.42º, 35.73º, 52.58º and 59.0º and hence the crystallinity of the CZS is found to be 77%. In XRD pattern of the TFL/CZS nanoparticles (Fig. 6c), the peaks at 16.7º, 22.07º, 28.11º, 33.42º, 35.73º, 52.58º and 59.0º disappeared, suggesting that the original CZS phases are no longer present alone [28,29]. Instead, new peaks appear at 12.01º, 21.22º, 24.53º, 29.64º, 38.10º and 41.29º, showing significant changes in the intensity and possibly new phases in the composite might have formed by incorporation of metals and organic moiety (Fig. 6). Also the crystallinity of TFL/CZS nanoparticles was found near 62% which clearly indicate that the crystallinity range of obtained nanoparticles *i.e.* TFL/CZS is between TFL and CZS. The disappearance of these peaks and the appearance of new peak indicate the immersion of the CZS component into TFL matrix, which is responsible for alteration of the crystalline structure [30,31]. Quantification of XRD peak intensities was conducted by calculating full width at half maximum (FWHM), peak are and intensity ratios for the different phases. Statistical analysis was performed to evaluate the significant variations in peak intensities and crystallinity percentages across samples.

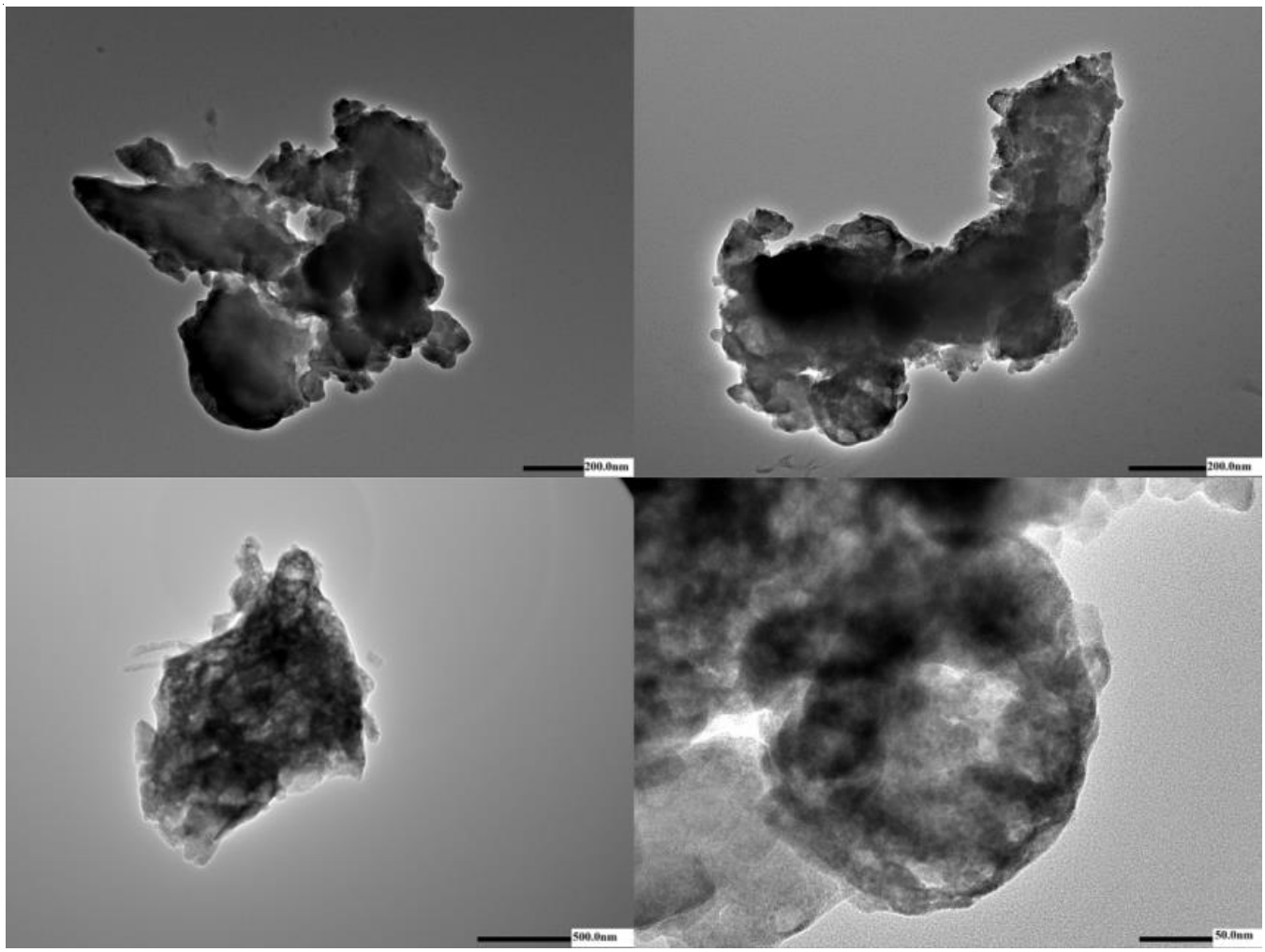

Fig. 5. TEM images of TFL/CZS at different magnifications

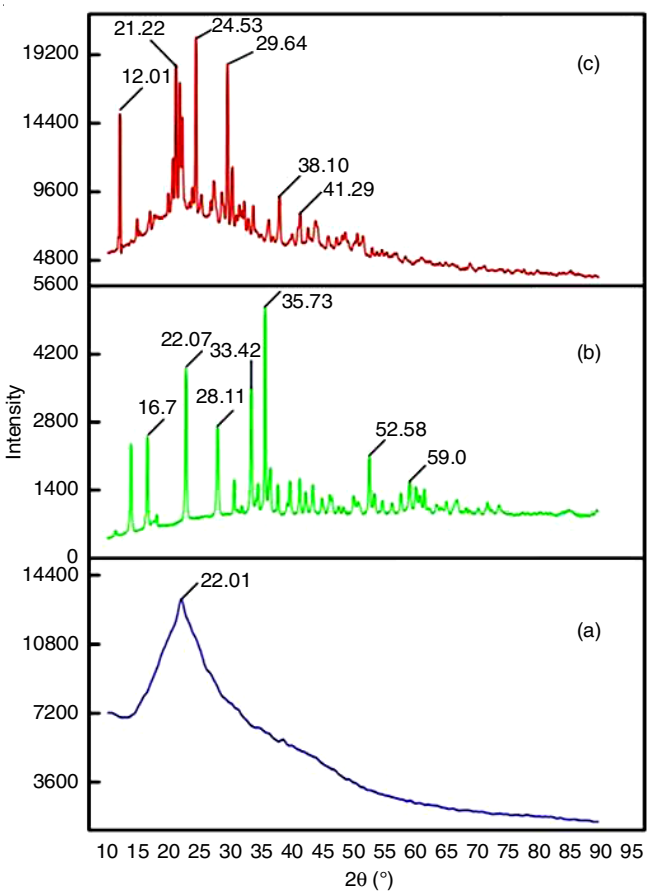

Fig. 6. XRD pattern of (a) leaf powder *i.e.* TFL, (b) inorganic salts *i.e.* Cu-Zn and (c) bi-metallic nanoparticles *i.e.* TFL/CZS

The Debye-Scherrer's formula was used to calculate the crystallite size from XRD data as:

$$D = \frac{K\lambda}{\beta\cos\theta}$$

where D = crystallite size (in nm), K = shape factor (typically 0.89 for spherical particles), λ = X-ray wavelength (depends on the X-ray source), β = full width at half maximum (FWHM) of the peak (in radians), θ = Bragg angle (the diffraction angle, in degrees).

Biological activities: Evaluation of antimicrobial activity of TFL/CZS nanoparticles was conducted by observing the inhibition zone against two strains of bacteria *i.e. S. typhi* and *B. subtilis* along with two strains of fungi *i.e. A. niger* and *E. nigrum.* The extent of antimicrobial activity and effect of concentration was verified by preparing solutions of different concentrations such as 10, 25, 50 and 100 µg/mL. The MIC of TFL/CZS were observed at 14 µg/mL. The antimicrobial activity evaluated at different concentrations of TFL/CZS nanoparticles was also compared with the standard drugs *i.e.* neomycin and fluconazole (15 µg/mL). The results revealed that the synthesized nanoparticles showed excellent antimicrobial activity against both bacterial and fungal strains. The inhibition zones (mm) of varying sizes were obtained as mentioned in Table-2. The zone of inhibition for 100 µL TFL/CZS nanoparticles solution was found to very close that has been exhibited by standard drugs *i.e.* (21.5 ± 0.4-0.7) and (20 ± 0.4-0.7) for bacterial strains and (19 ± 0.4-0.7) and (21 ± 0.4-0.7) for fungal strains.

Anti-angiogenic activity: The chicken chorioallantoic membrane (CAM) is an economical, simple and commonly used method to find the initial screening in the form of potential inhibitors of angiogenesis. In this study, two eggs were used to evaluate the ability of synthesized nanoparticles to hinder the origination of blood vessels on CAM has shown in Fig. 7. The percentage of inhibition of vessel growth rate in TFL/CZS nanoparticles treated groups were 28% (1 µg/mL) and 85% (10 µg/mL) in comparison with control [32,33]. The results revealed that synthesized nanoparticles has potential to stop the growth of neo-vascularization on CAM hence may act as excellent anticancer agent.

Photodegradation studies: The photodegradation activity of TFL/CZS nanoparticles was examined for Congo red dye in sunlight irradiation. Fig. 8a-b depicts the UV photodegradation spectra of Congo red dye at regular time intervals of sunlight exposure with TFL/CZS and CZS, respectively. The peak intensity decreases with increase in exposure time showing decrease in the concentration of Congo red. Fig. 8c depicts the % degradation of Congo red dye. The% degradation found to be 83% for TFL/CZS and 53% for CZS nanoparticles. The photodegradation process follows pseudo first-order kinetics as shown in Fig. 8d. The rate constant value for TFL/CZS was found to be 0.0027636 min^{-1} and 0.0147392 min^{-1} for CZS (Table-3) [34]. The enhanced photoactivity of TFL/CZS may be due to the formation of suitable band gap energies, decrease in recombination of photogenerated ions, synergetic association of TFL/CZS. This efficiently increases the absorption of visible light.

TABLE-3
RATE AND HALF-LIFE PERIOD VALUES OF PHOTO DEGRADATION REACTION OF CONGO RED

Sample	Rate (min^{-1})	Half-life period (min)
TFL/CZS	0.0027636	30.39513678
CZS	0.0147392	47.01747720

The effect of pH on the removal of Congo red in presence of TFL/CZS and CZS was studied in the pH range 3-11 and plots are shown in Fig. 9a-b. The results tabulated in Table-4

TABLE-2
INHIBITION ZONES (mm, n = 3) OF NANOPARTICLES AGAINST BACTERIAL AND FUNGAL SPECIES

Microorganism		Concentration (µg/mL)			Positive control (µg/mL)
		25	50	100	15
Bacteria	*Salmonella typhi*	12 ± 0.5	16 ± 0.7	21.5 ± 0.4	23 ± 0.5
	Bacillus subtilis	13 ± 0.6	16 ± 0.5	20 ± 0.5	23 ± 0.6
Fungi	*Epicoccum nigrum*	10 ± 0.7	13 ± 0.6	19 ± 0.4	20 ± 0.5
	Aspergillus niger	11 ± 0.5	13 ± 0.4	20 ± 0.7	21 ± 0.4

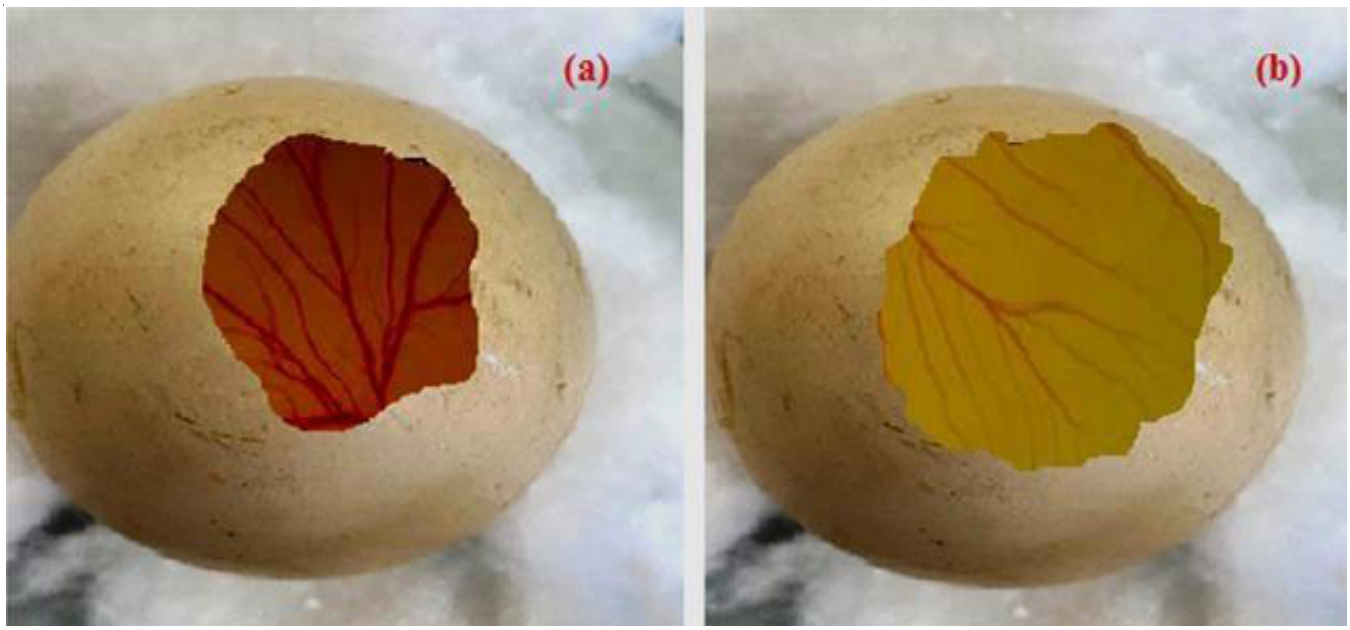

Fig. 7. Anti-angiogenic activity shown by (a) TFL (b) TFL/CZS at 1 µg/mL

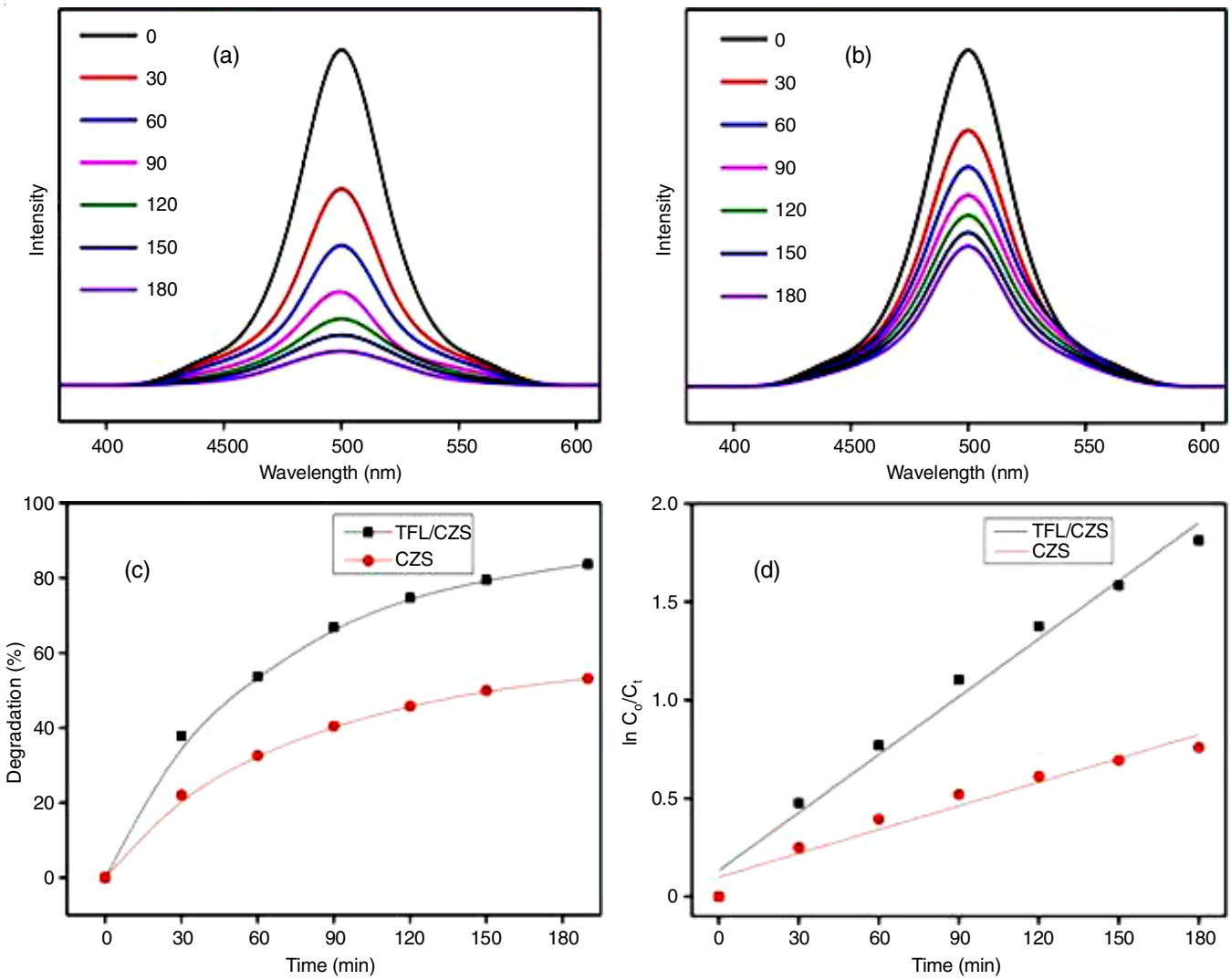

Fig. 8. UV spectrum of (a) TFL/CZS, (b) CZS with Congo red (c) % degradation of TFL/CZS and CZS (d) ln C_o/C_t *vs.* time with Congo red

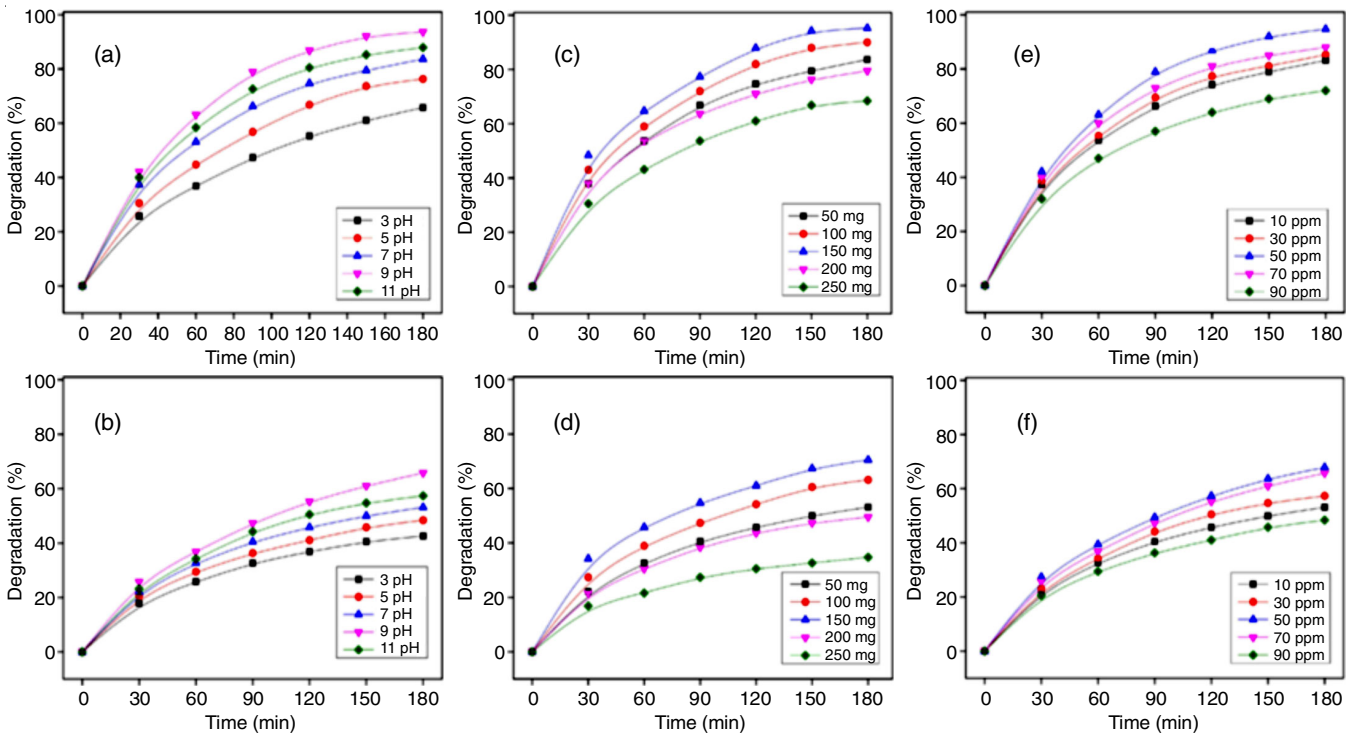

Fig. 9. Effect of pH on % degradation of (a) TFL/CZS and (b) CZS with Congo red. Effect of catalyst loading on% degradation of Congo red with (c) TFL/CZS (d) ZCS. Effect of concentration of Congo red on % degradation of (e) TFL/CZS and (f) CZS

TABLE-4
RATE CONSTANT (min^{-1}) AND HALF TIME PERIOD (min) OF DIFFERENT PARAMETERS IN PHOTO DEGRADATION PROCESS

	Congo red								
	pH			Dye concentration			Catalyst loading		
TFL/CZS	3 pH	.0133	51.88	10 ppm	.0223	31.02	50 mg	.0225	33.70
CZS		.0066	103.76		.0092	75.22		.0092	75.22
TFL/CZS	5 pH	.0186	37.14	30 ppm	.0241	28.65	100 mg	.0223	31.02
CZS		.0080	85.97		.0105	65.41		.0124	55.72
TFL/CZS	7 pH	.0227	30.39	50 ppm	.0391	17.70	150 mg	.0400	17.29
CZS		.0092	75.22		.0140	49.32		.0147	47.01
TFL/CZS	9 pH	.0363	19.04	70 ppm	.0262	26.39	200 mg	.0195	35.40
CZS		.0133	51.88		.0133	51.88		.0082	83.58
TFL/CZS	11 pH	.0271	25.50	90 ppm	.0204	33.81	250 mg	.0145	47.76
CZS		.0105	65.41		.0080	85.97		.0050	136.77

showed that at pH 9 maximum degradation rate 43.86075949 min^{-1} for TFL/CZS (51.88135416 min^{-1} for CZS) was observed. The rate values at different catalyst concentration are shown in Table-4. For Congo red dye, Fig. 9c-d shows the effect of catalyst loading on the % degradation of dye with TFL/CZS and CZS. The maximum rate of Congo red dye degradation was 0.0400 min^{-1} with 150 mg of TFL/CZS loading and 0.0147 min^{-1} with 150 mg of CZS loading. As the dosages amount increased above 150 mg L^{-1}, the rate start to decrease because the higher concentration of catalyst block the passage of light as a result of which efficacy of overall degradation process get declined [35-37]. The rate of removal of Congo red dye was maximum 0.0391 min^{-1} with TFL/CZS (0.0140 min^{-1} with CZS) for 50 ppm of dye concentration (Fig. 9e-f). As the concentration of Congo red increases the rate decreases. The decline is due to the lack of active sites with increase in Congo red dye concentration [38]. All active sites get saturated and hinder the photodegradation process.

Conclusion

A simple and economical approach for the synthesis of bimetallic (Cu-Zn) nanoparticles using *Trifolium alexandrinum* leaf extract is achieved. The green method employed minimal chemicals, making it eco-friendly and sustainable. The information of TFL/CZS nanoparticles was confirmed through spectral and analytical techniques, including FTIR, SEM, TEM, XRD and EDX, with changes in colour and spectral data indicating successful synthesis. The bimetallic nanoparticles exhibited significant antimicrobial and anti-angiogenic activities, with inhibition percentage quantified for angiogensis suppression. The photocatalytic potential of nanoparticles was tested against Congo red dye, demonstrating an % degradation rate at different concentrations and time intervals, proving their effective-ess in the wastewater treatment. Furthermore, the crystallinity analysis (XRD) also confirmed the structural stability of synthesized bimetallic (TFL/CZS) nanoparticles exhibiting 62% crystallinity.

CONFLICT OF INTEREST

The authors declare that there is no conflict of interests regarding the publication of this article.

REFERENCES

1. K.A. Altammar, *Front. Microbiol.*, **14**, 1155622 (2023); https://doi.org/10.3389/fmicb.2023.1155622
2. B. Pelaz, S. Jaber, D.J. de Aberasturi, V. Wulf, T. Aida, J.M. de la Fuente, J. Feldmann, H.E. Gaub, L. Josephson, C.R. Kagan, N.A. Kotov, L.M. Liz-Marzán, H. Mattoussi, P. Mulvaney, C.B. Murray, A.L. Rogach, P.S. Weiss, I. Willner and W.J. Parak, *ACS Nano*, **6**, 8468 (2012); https://doi.org/10.1021/nn303929a
3. J. Ramsden, Nanotechnology: An Introduction, William Andrew (2016).
4. M. Herlekar, S. Barve and R. Kumar, *J. Nanoparticles*, **1**, 140614 (2014); https://doi.org/10.1155/2014/140614
5. S. Frank and S. Schilthuizen, Nanotechnology; Innovation Opportunities for Tomorrow's Defence; TNO Science & Industry Future Technology Center: The Netherlands (2006).
6. H. Duan, D. Wang and Y. Li, *Chem. Soc. Rev.*, **44**, 5778 (2015); https://doi.org/10.1039/C4CS00363B
7. N. Bala, S. Saha, M. Chakraborty, M. Maiti, S. Das, R. Basu and P. Nandy, *RSC Adv.*, **5**, 4993 (2015); https://doi.org/10.1039/C4RA12784F
8. J.S. Moodley, S.B.N. Krishna, K. Pillay, Sershen and P. Govender, *Adv. Nat. Sci. Nanosci. Nanotechnol.*, **9**, 015011 (2018); https://doi.org/10.1088/2043-6254/aaabb2
9. I.-M. Chung, A. Abdul Rahuman, S. Marimuthu, A. Vishnu Kirthi, K. Anbarasan, P. Padmini and G. Rajakumar, *Exp. Ther. Med.*, **14**,18 (2017); https://doi.org/10.3892/etm.2017.4466
10. J. Suresh, G. Pradheesh, V. Alexramani, M. Sundrarajan and S.I. Hong, *Adv. Nat. Sci.: Nanosci. Nanotechnol.*, **9**, 015008 (2018); https://doi.org/10.1088/2043-6254/aaa6f1
11. G. Sharma, A. Kumar, S. Sharma, M. Naushad, R. Prakash Dwivedi, Z.A. ALOthman and G.T. Mola, *J. King Saud Univ. Sci.*, **31**, 257 (2019); https://doi.org/10.1016/j.jksus.2017.06.012
12. P. Kuppusamy, M.M. Yusoff, G.P. Maniam and N. Govindan, *Saudi Pharm. J.*, **24**, 473 (2016); https://doi.org/10.1016/j.jsps.2014.11.013
13. A.V. Khan, Q.U. Ahmed, I. Shukla and A.A. Khan, *Asian Pac. J. Trop. Biomed.*, **2**, 189 (2012); https://doi.org/10.1016/S2221-1691(12)60040-9
14. T. Sabudak and N. Guler, *Phytother. Res.*, **23**, 439 (2009); https://doi.org/10.1002/ptr.2709
15. M. Sharaf, *Nat. Prod. Res.*, **22**, 1620 (2008); https://doi.org/10.1080/14786410701869226
16. G. Blunden, *Phytother. Res.*, **15**, 89 (2001); https://doi.org/10.1002/ptr.982
17. M. Li, H. Yu, Y. Cheng, Y. Guo, W. Yao and Y. Xie, *Ecotoxicol. Environ. Saf.*, **200**, 110780 (2020); https://doi.org/10.1016/j.ecoenv.2020.110780
18. L. Trotsiuk, A. Antanovich, A. Lizunova and O. Kulakovich, *Colloid Interface Sci. Commun.*, **37**, 100289 (2020); https://doi.org/10.1016/j.colcom.2020.100289
19. B. Naiel, M. Fawzy, M.W.A. Halmy and A.E.D. Mahmoud, *Sci. Rep.*, **12**, 20370 (2022); https://doi.org/10.1038/s41598-022-24805-2
20. L.C. Ann, S. Mahmud, S.K.M. Bakhori, A. Sirelkhatim, D. Mohamad, H. Hasan, A. Seeni and R.A. Rahman, *AIP Conf. Proc.*, **1657**, 100012 (2015); https://doi.org/10.1063/1.4915219
21. C.B. Adamo, A.S. Junger, L.P. Bressan, J.A.F. da Silva, R.J. Poppi and D.P. de Jesus, *Microchem. J.*, **156**, 104985 (2020); https://doi.org/10.1016/j.microc.2020.104985
22. B. Marina, M. Giovanela, M. Roesch-Ely, M. Devine and J.D.S. Crespo, *Sustain. Chem. Pharm.*, **15**, 100223 (2020); https://doi.org/10.1016/j.scp.2020.100223
23. M. Ganesh, S.G. Lee, J. Jayaprakash, M. Mohankumar and H.T. Jang, *Biocatal. Agric. Biotechnol.*, **19**, 101129 (2019); https://doi.org/10.1016/j.bcab.2019.101129
24. D. Hu, W.B. Si, W. Qin, J. Jiao, X.L. Li, X.P. Gu and Y.F. Hao, *J. Photochem. Photobiol. B*, **195**, 12 (2019); https://doi.org/10.1016/j.jphotobiol.2019.04.001
25. C. Changchun, B. Yu, P. Liu, J.F. Liu and L. Wang, *J. Ceram. Process. Res.*, **12**, 420 (2011); https://doi.org/10.36410/jcpr.2011.12.4.420
26. J. Lu, I. Batjikh, J. Hurh, Y. Han, H. Ali, R. Mathiyalagan, C. Ling, J.C. Ahn and D.C. Yang, *Optik*, **182**, 980 (2019); https://doi.org/10.1016/j.ijleo.2018.12.016
27. M.B. Muradov, S.J. Mammadyarova, G.M. Eyvazova, O.O. Balayeva, G. Aliyeva, I. Hasanova, S.Z. Melikova, N. Musayeva, N. Sadigov and M.I. Abdullayev, *RSC Adv.*, **14**, 1082 (2024); https://doi.org/10.1039/D2RA08060E
28. B.D. Cullity and R. Smoluchowski, *Phys. Today*, **10**, 50 (1957); https://doi.org/10.1063/1.3060306
29. B.E. Warren, X-ray Diffraction, Addison-Wesley Publishing Company (1969).
30. P.K. Harold and L.E. Alexander, X-ray Diffraction Procedures for Polycrystalline and Amorphous Materials, Wiley-Interscience, pp. 228-235 (1955).
31. R. Jenkins and R.L. Snyder, Introduction to X-ray Powder Diffractometry, Wiley Interscience (1996).
32. H. Zarharan, M. Bagherian, A. Shah-Rokhi, R.R. Bajgiran, E. Yousefi, P. Heravian, M.N. Khazrabig, A. Es-haghi and M.E. Taghavizadeh Yazdi, *Arab. J. Chem.*, **16**, 104806 (2023); https://doi.org/10.1016/j.arabjc.2023.104806
33. S.R. Kumar, C.-C. Hu, T.T.T. Vi, D.W. Chen and S.J. Lue, *Antibiotics*, **12**, 1407 (2023); https://doi.org/10.3390/antibiotics12091407
34. L. Xingqi and L. Cai, *Appl. Surf. Sci.*, **483**, 875 (2019); https://doi.org/10.1016/j.apsusc.2019.03.273
35. M.R. Abhilash, G. Akshatha and S. Srikantaswamy, *RSC Adv.*, **9**, 8557 (2019); https://doi.org/10.1039/C8RA09929D
36. M.H. Habibi, A. Hassanzadeh and S. Mahdavi, *J. Photochem. Photobiol. Chem.*, **172**, 89 (2005); https://doi.org/10.1016/j.jphotochem.2004.11.009
37. U.G. Akpan and B.H. Hameed, *J. Hazard. Mater.*, **170**, 520 (2009); https://doi.org/10.1016/j.jhazmat.2009.05.039
38. N. Yahya, F. Aziz, J. Jaafar, W.J. Lau, N. Yusof, W.N.W. Salleh, A.F. Ismail and M. Aziz, *Arab. J. Sci. Eng.*, **46**, 6153 (2021); https://doi.org/10.1007/s13369-020-04874-z